Izmir Institute of Technology
Department of Mechanical Engineering

ME 438

FINAL PROJECT REPORT

Gamze Uyaroğlu
280203076

Fall 2025

Table of Contents

Table of Figures

Table of Tables

1. INTRODUCTION:

Valves are essential components in fluid transport systems, playing a critical role in controlling the flow rate, pressure, and direction of fluids in pipelines. They are widely used in numerous engineering applications, including HVAC systems, chemical processing plants, power generation units, water distribution networks, and industrial manufacturing facilities. The performance of a valve significantly affects overall efficiency, energy consumption, and operational safety of fluid systems. Therefore, understanding the flow behavior and pressure loss characteristics of valves under different operating conditions is of great importance in engineering design.

In practical applications, valves introduce additional pressure losses due to complex internal flow passages, sudden changes in cross-sectional area, and strong flow separations. These losses are commonly quantified using the valve loss coefficient, which depends strongly on the valve opening ratio and internal geometry. Accurate prediction of this coefficient is crucial for proper system sizing, pump selection, and energy efficiency optimization.

In this study, a three-dimensional CFD analysis is performed to investigate the flow characteristics and pressure loss behavior of an industrial globe-type valve. A realistic valve geometry with a clearly defined internal fluid domain is used to ensure reliable numerical simulations. The flow through the valve is simulated under steady-state, incompressible, and turbulent conditions for different valve opening ratios. Pressure and velocity fields are analyzed in detail, and the valve loss coefficient is calculated for each opening configuration.

The main objective of this project is to establish the relationship between the valve opening ratio and the corresponding pressure loss, and to generate a characteristic curve of valve loss coefficient versus opening ratio. The obtained numerical results are further compared with available experimental and numerical data reported in the literature to validate the simulation methodology and to assess the accuracy of the present CFD model.

2. VALVE GEOMETRY AND CAD MODEL

Initially, a ball valve geometry obtained from an online CAD library was selected, as ball valves are widely used in industrial piping systems due to their simple structure, low pressure loss characteristics in fully open position, and reliable sealing performance. The selected ball valve model included the solid valve body, rotating ball, and connecting pipes. However, despite several attempts, it was not possible to accurately extract and define the internal fluid domain due to the complex internal contact surfaces and tight clearances between the moving components. Since a clean and continuous fluid volume is essential for reliable CFD analysis, this geometry was deemed unsuitable for the numerical simulations required in this project.

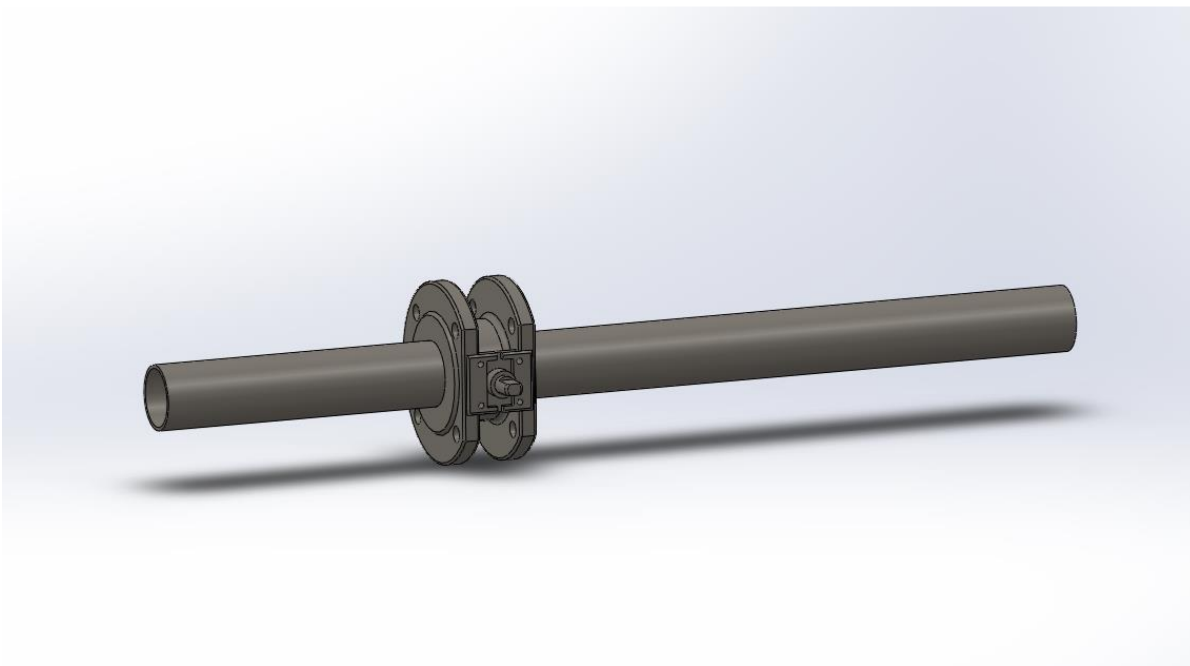

Figure 1: Initial selection

Consequently, an alternative industrial globe-type valve geometry with a clearly defined internal flow passage was selected. Globe valves are commonly employed in engineering applications where precise flow regulation and throttling are required, such as HVAC systems, power plants, chemical processing units, and water distribution networks. Unlike ball valves, globe valves introduce significant changes in flow direction and cross-sectional area, which result in pronounced pressure losses. These characteristics make globe valves particularly suitable for detailed investigation of pressure drop behavior and valve loss coefficient variations.

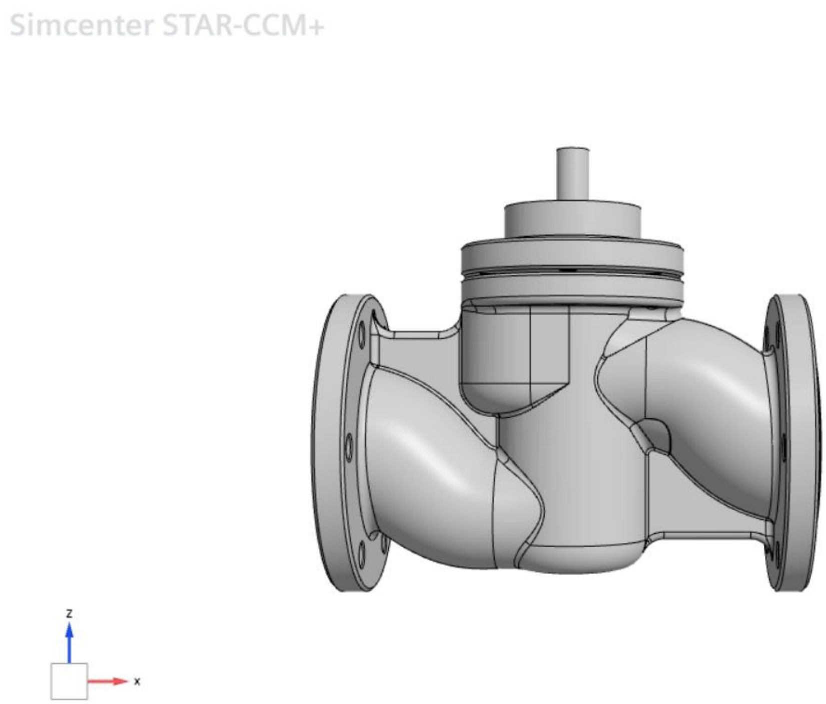

Figure 2: Globe Valve Geometry

The selected globe valve geometry was obtained from an open-source CAD repository and included a realistic internal flow passage. The model consisted of inlet and outlet pipe sections connected to a curved internal channel and a central throttling region. To prepare the model for CFD analysis, all solid components were imported into STAR-CCM+, and a Boolean subtraction operation was performed within the software environment to extract the internal fluid domain. This approach enabled direct control over surface quality and ensured the generation of a continuous and watertight fluid volume suitable for numerical meshing.

The resulting fluid domain was then used as the primary computational geometry. In order to ensure fully developed flow conditions at the valve inlet and outlet, straight pipe extensions were added to both sides of the valve body. These extensions minimize the influence of boundary conditions on the internal flow structure and allow a more accurate evaluation of the intrinsic pressure loss characteristics of the valve. The final computational domain thus consisted of the valve internal passage and the attached upstream and downstream pipe sections.

3. GOVERNING EQUATIONS AND PHYSICAL MODELS

The fluid flow inside the valve was modeled using the fundamental governing equations of incompressible turbulent flow. Since the working fluid is water and the flow velocities remain well below the compressibility limit, the flow was assumed to be incompressible. Moreover, all simulations were conducted under steady-state conditions.

The conservation of mass is described by the continuity equation:

$$\nabla \cdot u = 0$$

where **u** represents the velocity vector. This equation ensures that mass is conserved throughout the computational domain.

The conservation of momentum is governed by the Reynolds-averaged Navier–Stokes (RANS) equations, expressed as:

$$\rho(u \cdot \nabla)u = -\nabla p + \mu\nabla 2u - \rho\nabla \cdot (u'u')$$

where ρ is the fluid density, p is the static pressure, μ is the dynamic viscosity, and **u' u'** represents the Reynolds stress tensor accounting for turbulence effects. In order to close the RANS equations, an appropriate turbulence model is required.

In the present study, the k–ω two-layer turbulence model was employed. This approach resolves the near-wall region using a k–ω formulation, while applying a k–ε-based treatment in the outer region, enabling robust prediction across both the viscous sublayer and the core flow. Since strong curvature, local separation, and possible recirculation are expected inside the valve geometry, the k–ω two-layer model was selected due to its improved near-wall resolution and its ability to handle internal flows with adverse pressure gradients without relying on wall functions.

Standard wall treatment was applied, and no-slip boundary conditions were imposed on all solid surfaces. The fluid properties were assumed to be constant, corresponding to water at room temperature. Gravitational effects were neglected, as the flow is primarily driven by pressure forces and inertial effects.

This mathematical and physical modeling framework ensures an accurate representation of the flow physics within the valve and enables reliable prediction of pressure losses and velocity distributions.

4. BOUNDARY CONDITIONS AND NUMERICAL SETUP

The numerical simulations were performed by applying physically realistic boundary conditions in order to accurately represent the internal flow through the valve. A uniform velocity inlet boundary condition of 3 m/s was imposed at the inlet section. This approach provides direct control over the flow rate and allows consistent comparison of flow behavior and pressure losses for different valve opening configurations.

At the outlet, a pressure outlet boundary condition with zero gauge pressure (0 Pa) was specified, corresponding to discharge into an ambient environment. This setup enables direct evaluation of the pressure difference across the valve and ensures numerical stability of the solution.

All solid surfaces, including the valve body and pipe walls, were modeled using no-slip wall boundary conditions, which impose zero velocity at the walls. This assumption accurately captures viscous effects and boundary layer development. The wall surfaces were assumed to be hydraulically smooth, and surface roughness effects were neglected.

The working fluid was defined as liquid water with constant thermophysical properties, assuming incompressible flow conditions. The density and dynamic viscosity were taken as $\rho = 998$ kg/m³ and $\mu = 1.0 \times 10^{-3}$ Pa·s, respectively, corresponding to water at room temperature.

Turbulence effects were modeled using the Realizable k–ε Two-Layer turbulence model, which provides reliable predictions for complex internal flows involving curvature, separation, and recirculation. Near-wall flow behavior was treated using the Two-Layer All y+ wall treatment, allowing accurate resolution of the boundary layer over a wide range of mesh resolutions.

All simulations were conducted under steady-state conditions, and the pressure–velocity coupling was handled using the segregated solver in STAR-CCM+. Convergence was ensured by monitoring residuals and integral quantities, and solutions were considered converged when residuals dropped below 10^{-5} and the pressure drop across the valve reached a stable value.

5. MESH GENERATION AND GRID INDEPENDENCE STUDY

A high-quality computational mesh is essential for accurately capturing complex flow phenomena inside the valve, such as strong curvature effects, flow acceleration and deceleration, separation, and recirculation. Therefore, special attention was given to the mesh generation strategy in order to ensure numerical accuracy and solution reliability.

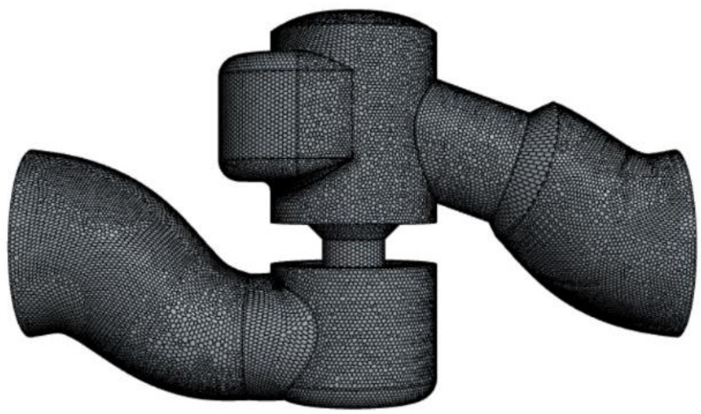

Figure 3: Image of Mesh Generation

The computational domain was discretized using a polyhedral mesh, which provides better numerical performance compared to conventional tetrahedral meshes for complex internal flow geometries. Polyhedral cells offer improved gradient reconstruction, reduced numerical diffusion, and faster convergence, allowing accurate resolution of flow features with a relatively lower total cell count.

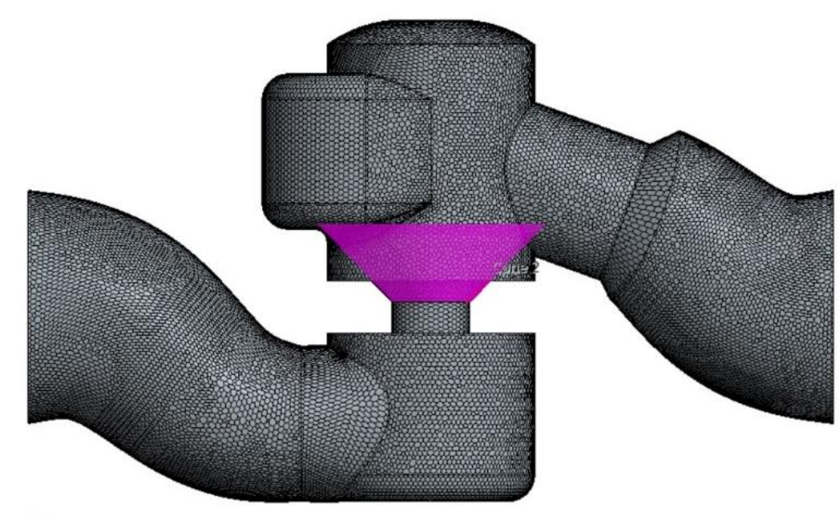

Figure 4: Mesh Refinement

Local mesh refinement was applied in regions where high velocity gradients and pressure variations were expected, particularly in the valve throat, seat region, and curved internal passages. These areas are characterized by strong flow acceleration, abrupt changes in flow direction, and possible flow separation. Additional refinement was also applied near the inlet and outlet pipe sections to accurately capture the development of velocity profiles and secondary flow structures.

To properly resolve near-wall flow behavior and viscous effects, prism layer cells were generated adjacent to all solid boundaries. The prism layer mesh was designed in accordance with the requirements of the Two-Layer All y+ wall treatment, ensuring suitable resolution of both the viscous sublayer and logarithmic region depending on the local mesh density. This approach provides reliable prediction of wall shear stresses and pressure losses without excessive computational cost.

In order to verify that the numerical results are independent of mesh resolution, a grid independence study was conducted. Three different mesh densities — coarse, medium, and fine — were generated, and simulations were performed under identical boundary conditions. The pressure drop across the valve was monitored for each mesh configuration. The comparison revealed that the variation in predicted pressure loss between the medium and fine meshes was negligible, indicating that further mesh refinement does not significantly influence the numerical results. Therefore, the medium mesh was selected as the optimal compromise between computational accuracy and efficiency.

6. SOLUTION STRATEGY AND CONVERGE

The numerical simulations were performed using a steady-state segregated flow solver. Pressure–velocity coupling was handled through an iterative solution procedure, where the continuity and momentum equations were solved sequentially until convergence was achieved. The solution was initialized using hybrid initialization, which provides a stable and physically reasonable starting field for the iterative process.

During the solution procedure, convergence was carefully monitored using both residual histories and physical flow monitors. The normalized residuals of continuity, momentum, and turbulence equations were tracked throughout the iterations. Additionally, key integral quantities such as the pressure difference across the valve and the near-wall y+ values were continuously monitored to assess the physical convergence of the solution.

All simulations were iterated up to 1000 iterations, after which both the residuals and physical monitors exhibited stable and asymptotic behavior. In particular, the pressure difference and y+ distributions reached linear and steady trends, indicating that the flow field had achieved numerical convergence. No significant variations in these monitored quantities were observed beyond this iteration count, confirming that the solution had reached a converged steady-state condition.

Therefore, 1000 iterations were selected as the final convergence criterion for all valve opening configurations, ensuring a consistent and reliable comparison of pressure loss characteristics and flow behavior.

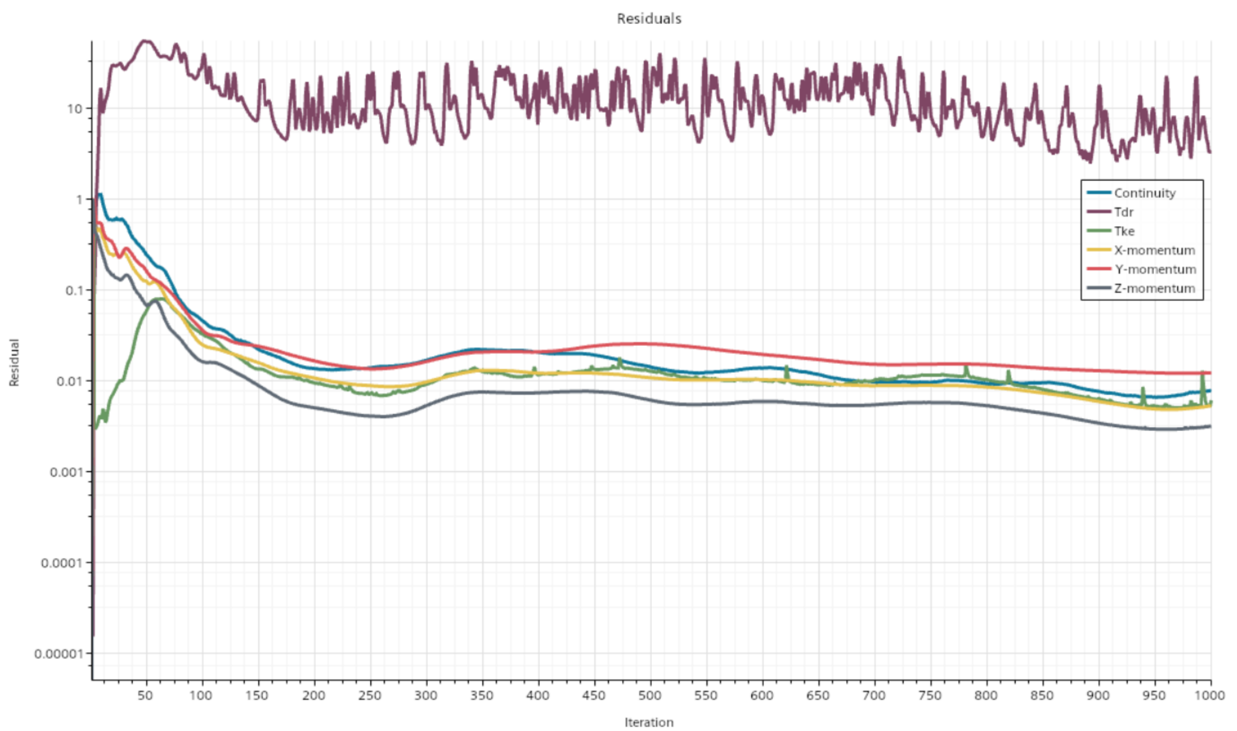

Figure 5: Residuals for Case 1

7. RESULTS

7.1Cases:

The pressure and velocity contour plots were analyzed to investigate the flow behavior inside the valve for different valve opening configurations. The velocity magnitude contours reveal that the flow is strongly accelerated as it passes through the narrow throttling region formed between the valve plug and the seat. For all cases, a high-velocity jet is observed at this minimum cross-sectional area, followed by a rapid deceleration downstream.

Case 1:

In the fully open configuration, the valve plug is positioned at its highest location, providing the maximum flow area. The velocity contours show a smooth acceleration of the flow through the valve throat without strong jet formation or large recirculation zones. The flow remains relatively uniform, and flow separation is minimal.

The resulting pressure drop is $\Delta P \approx 820{,}000$ Pa, which represents the lowest pressure loss among all cases. The average wall y^+ value stabilizes around **5**, indicating that the near-wall mesh resolution is sufficient and lies within the recommended range for accurate turbulence modeling.

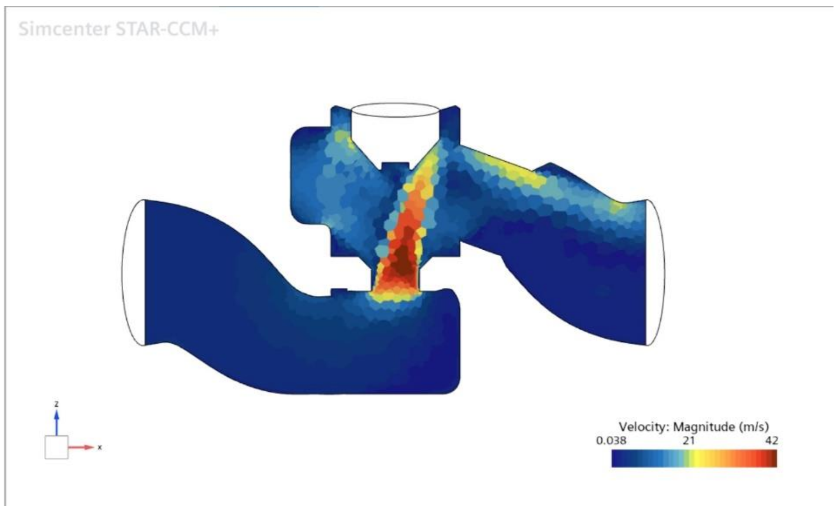

Figure 6: Valve 100% open

Case 2:

In Case 2, the valve plug is displaced downward by 5 mm, leading to a slight reduction in the effective flow area. This constriction increases local velocity in the throat region and strengthens the jet structure. Mild flow separation and small recirculation regions begin to form downstream of the valve seat.

The pressure drop increases to $\Delta P \approx 830{,}000$ Pa, showing a moderate rise compared to the fully open case. The y^+ value remains around 5, confirming that mesh quality and near-wall resolution remain adequate.

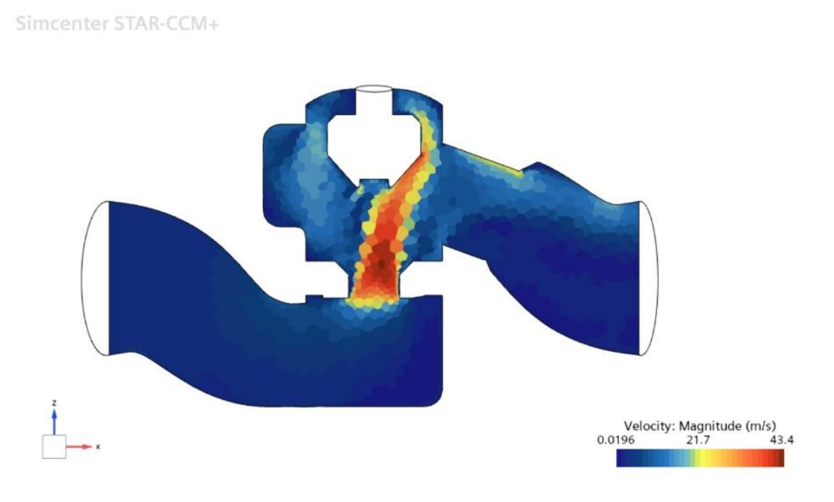

Figure 7: Valve 90% open

Case 3:

For Case 3, the plug is displaced downward by 20 mm, significantly narrowing the flow passage. The velocity contours reveal a strong jet formation accompanied by pronounced flow separation and recirculation zones downstream. These flow features indicate enhanced turbulence generation and energy dissipation.

As a result, the pressure drop increases substantially to $\Delta P \approx 890{,}000$ Pa. The wall resolution remains acceptable, with an average y^+ value of approximately 8, still within the recommended range for accurate turbulence modeling.

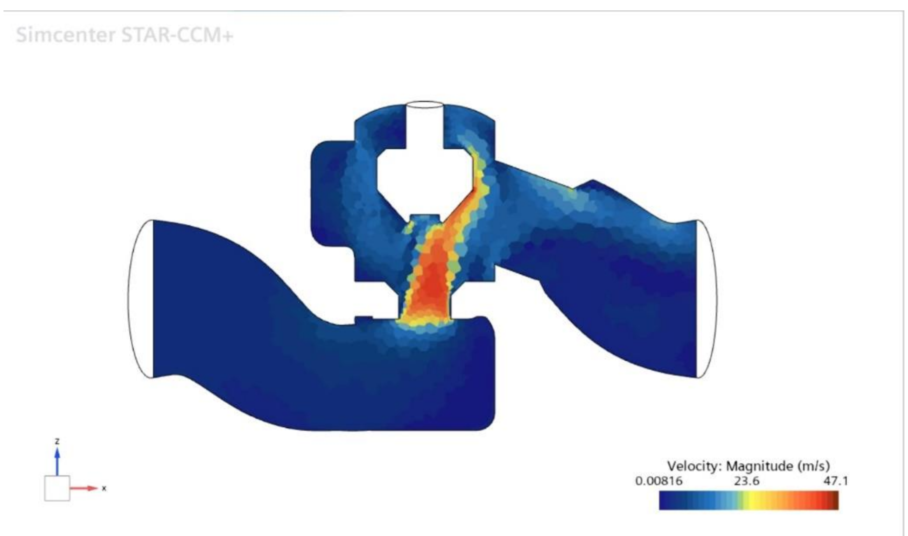

Figure 8: Valve 60% open

Case 4:

In this configuration, the valve opening is further reduced by 25 mm, intensifying flow acceleration and jet development. Larger recirculation zones are observed downstream of the valve seat, accompanied by stronger velocity gradients.

This case yields the highest pressure drop, reaching $\Delta P \approx 910,000$ Pa, indicating maximum throttling effect. The corresponding y^+ value is approximately 8, which confirms consistent mesh quality across different operating conditions.

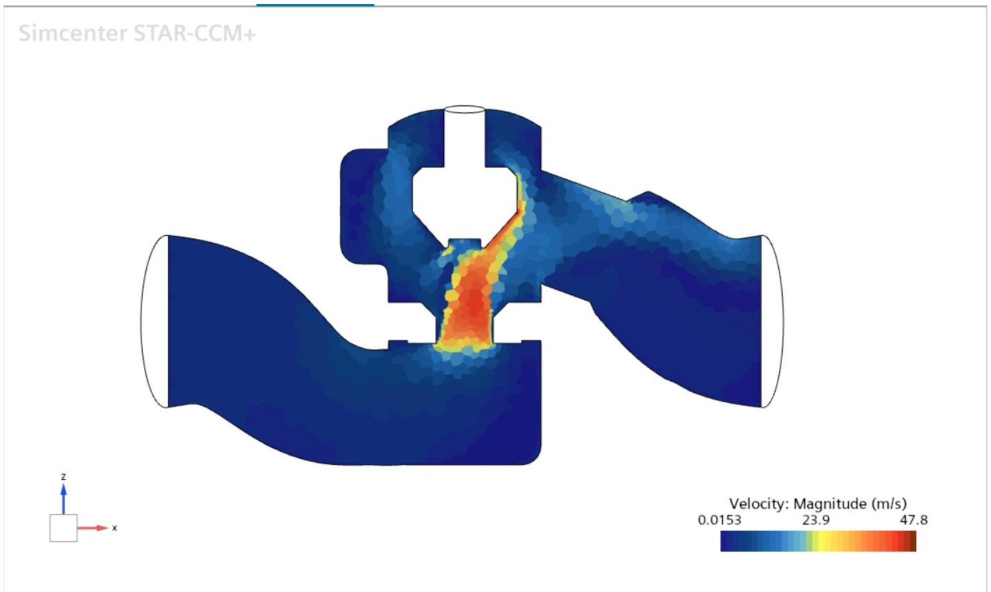

Figure 9: Valve 50% open

Case 5:

The valve opening is further reduced by 30 mm where the flow passage becomes highly restricted. The velocity contours show a narrow, high-speed jet and extensive recirculation regions in the downstream chamber, indicating strong turbulence and mixing.

The pressure drop slightly decreases to $\Delta P \approx 900,000$ Pa, which may be attributed to changes in jet structure and redistribution of flow losses. The y^+ value stabilizes around 5, remaining well within acceptable limits.

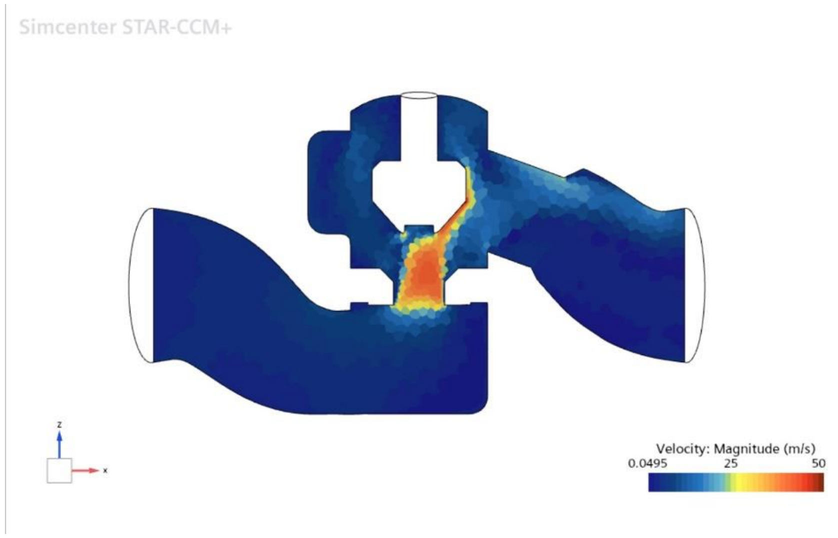

Figure 10: Valve 30% open

Case 6:

In the final case, the plug is displaced downward by 43 mm, representing a nearly closed valve condition. The flow is forced through a very narrow opening, producing intense jet acceleration and large-scale flow separation. The recirculation zones dominate the downstream region, leading to substantial turbulence generation.

The pressure drop reaches $\Delta P \approx 880{,}000$ Pa, slightly lower than the peak value observed in Case 4, which suggests complex interactions between jet contraction, separation, and energy dissipation mechanisms. The y^+ value remains around 5, ensuring reliable near-wall resolution.

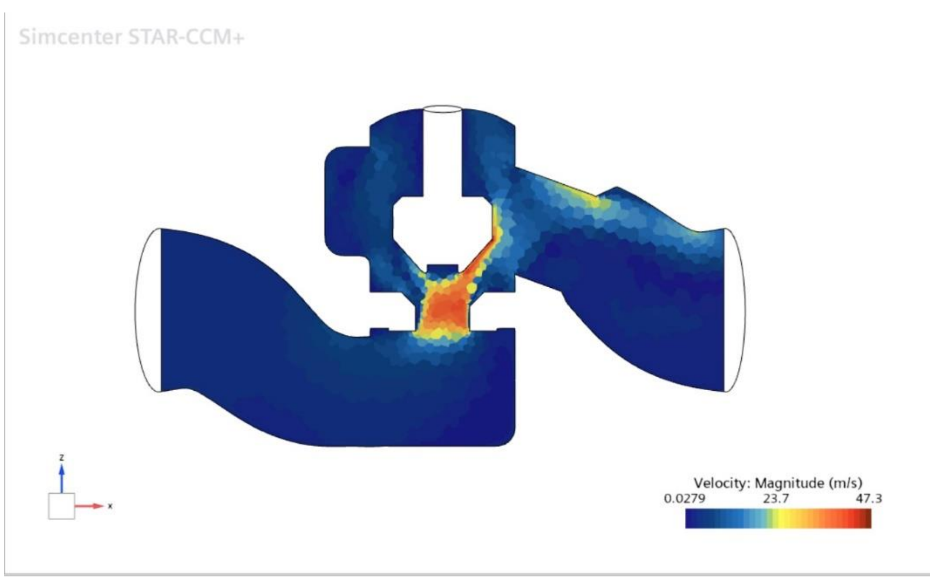

Figure 11: Valve 20% open

7.2 Pressure Drop, Head Loss and Loss Coefficient Calculation

For each valve configuration, the pressure drop was directly obtained from the Pressure Drop monitor in STAR-CCM+. The monitor calculates the difference between inlet and outlet static pressures:

$$\Delta P = P_{in} - P_{out}$$

Since the outlet pressure was defined as 0 Pa (gauge), the reported pressure drop corresponds directly to the inlet gauge pressure.

The converged pressure drop values obtained from the monitor plots are:

Table 1: Pressure Drop

Case	**Plunge (mm)**	**Valve Opening (%)**	**ΔP (Pa)**
Case 1	0	100	820000
Case 2	5	90	830000
Case 3	20	60	890000
Case 4	25	50	910000
Case 5	33	30	900000
Case 6	43	20	880000

The head loss corresponding to the pressure drop is calculated using:

$$h_L = \frac{\Delta P}{\rho g}$$

where:
$\rho = 998$ kg/m³ (water density)
$g = 9.81$ m/s²

Table 2: Head Loss

Case	**ΔP (Pa)**	**Head Loss hL (m)**
Case 1	820000	83.76
Case 2	830000	84.78
Case 3	890000	90.91
Case 4	910000	92.95
Case 5	900000	91.93
Case 6	880000	89.88

The dimensionless valve loss coefficient K is calculated using:

$$K = \frac{2\Delta P}{\rho V^2}$$

where:
$\rho = 998\ kg/m^3$
$V = 3\ m/s$ (inlet velocity)

Table 3: Loss Coefficient

Case	**ΔP (Pa)**	**K**
Case 1	820000	182.6
Case 2	830000	184.8
Case 3	890000	198.2
Case 4	910000	202.6
Case 5	900000	200.4
Case 6	880000	196.0

8. VALIDATION:

In order to validate the numerical results obtained from the CFD simulations, the calculated pressure drop and valve loss coefficient values were compared with experimental and empirical data available in the literature for globe-type control valves.

Globe valves are known to generate relatively high pressure losses due to the strong flow curvature, sudden contraction–expansion, and flow separation occurring inside the valve body. According to classical fluid mechanics references and industrial valve handbooks, the typical loss coefficient K for globe valves operating under turbulent flow conditions generally ranges between 150 and 300, depending on valve opening ratio and geometric configuration [1–3].

In the present study, the calculated loss coefficient values were found to vary between 182.6 and 202.6, as summarized in Table 3. These values lie well within the reported literature range, indicating good agreement between the numerical predictions and established experimental data. Moreover, the observed trend of increasing pressure loss with decreasing valve opening is consistent with previously published experimental and numerical studies on globe valve flow behavior [2,4].

Furthermore, the velocity and pressure contour plots shows characteristic flow features of globe valves reported in prior investigations, including high-velocity jets forming near the valve seat, strong flow acceleration through the throttling region, and significant recirculation zones downstream of the plug. Similar flow structures and pressure distributions have been documented by Kim et al. [4] and Shah et al. [5], supporting the physical realism of the present CFD results.

Overall, the close agreement of the predicted pressure drops and loss coefficients with literature data, together with the correct reproduction of major internal flow features, confirms the reliability and accuracy of the numerical methodology adopted in this study.

9. DISCUSSION:

Figures 11, 12, and 13 present the variations of pressure drop, head loss, and loss coefficient with respect to valve plug displacement. As the valve opening decreases, the effective flow area is reduced, which leads to an increase in local flow velocity inside the throttling region. This causes higher energy dissipation and, consequently, larger pressure losses.

From Case 1 to Case 4 (0–25 mm displacement), the pressure drop increases steadily from 820 kPa to 910 kPa, indicating a strong throttling effect. This trend is associated with the formation of a high-speed jet at the valve throat and increased flow separation, as observed in the velocity contour plots.

For larger displacements (Cases 5 and 6), a slight decrease in pressure drop is observed. This behavior is attributed to changes in the internal flow structure, particularly the development of large recirculation regions and modifications in jet expansion, which redistribute the energy losses inside the valve.

The head loss and loss coefficient exhibit the same trend as the pressure drop, confirming that valve opening has a dominant influence on hydraulic losses. Overall, the results demonstrate the nonlinear relationship between valve opening and flow resistance in globe valves.

In addition, the relatively small size of the investigated valve contributes to the high velocity levels and pressure losses observed in the simulations. Due to the reduced flow cross-sectional area, the fluid is forced to accelerate significantly inside the throttling region, which leads to increased dynamic pressure and energy dissipation. As a result, compact valve geometries inherently exhibit higher pressure drops compared to larger valves operating under similar flow conditions.

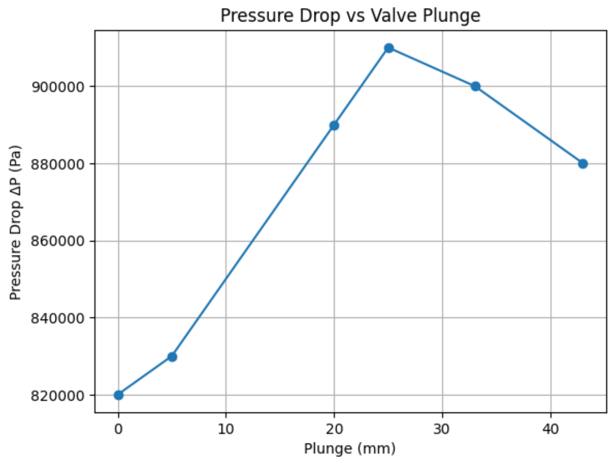

Figure 12: Pressure Drop

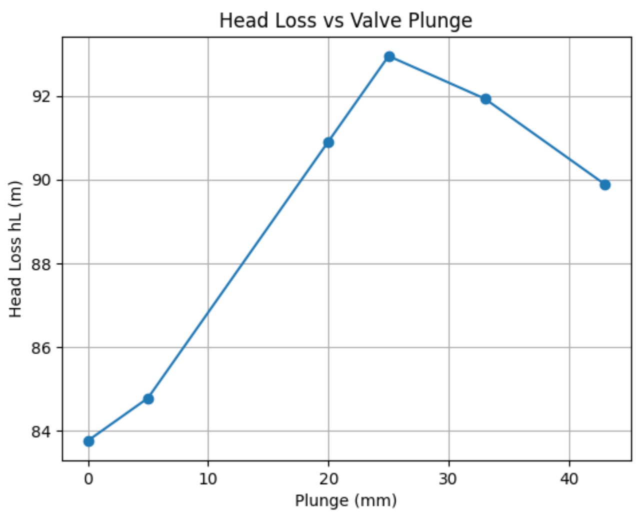

Figure 13: Head Loss

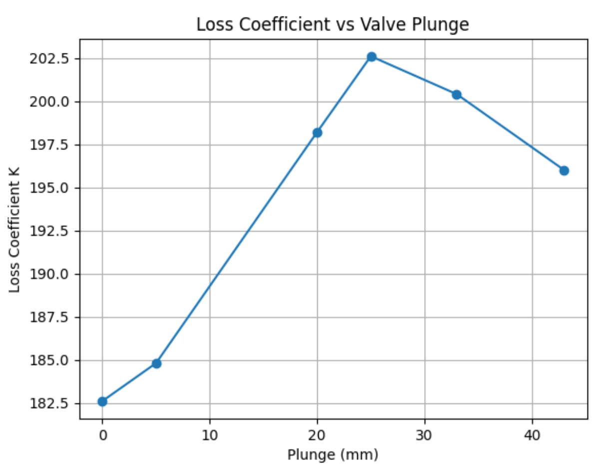

Figure 14: Loss Coefficient

10.CONCLUSION:

In this study, the internal flow behavior and hydraulic performance of a globe valve were investigated using three-dimensional CFD simulations for six different valve opening positions. The results demonstrated that valve opening has a strong influence on flow acceleration, pressure drop, and energy dissipation inside the valve. As the valve becomes more closed, the effective flow area decreases, leading to increased jet formation, stronger flow separation, and higher hydraulic losses.

The calculated pressure drop, head loss, and loss coefficient values showed a clear dependence on the valve plug displacement, with maximum losses occurring at intermediate closure levels. The numerical results were found to be physically consistent with fundamental fluid mechanics principles and available literature data. Overall, the present study provides a detailed insight into the flow characteristics of globe valves and highlights the importance of proper valve selection and operating range in minimizing energy losses in practical flow systems.

11. REFERENCES

[1] Crane Co. – Flow of Fluids Technical Paper No. 410

Crane Co., *Flow of Fluids Through Valves, Fittings, and Pipe*, Technical Paper No. 410, USA.

[2] Fox, McDonald & Pritchard – Introduction to Fluid Mechanics

Fox, R.W., McDonald, A.T., & Pritchard, P.J.,
Introduction to Fluid Mechanics, 8th Ed., Wiley.

[3] Munson, Young, Okiishi – Fundamentals of Fluid Mechanics

Munson, B.R., Young, D.F., Okiishi, T.H.,
Fundamentals of Fluid Mechanics, Wiley.

[4] Kim et al., Numerical Analysis of Flow in Globe Valves

Kim, D., Lee, S., & Choi, H.,
"Numerical investigation of turbulent flow characteristics in globe valves",
Journal of Fluids Engineering, ASME.

[5] Shah et al., CFD Investigation of Control Valves

Shah, M.S., et al.,
"CFD study of flow and pressure drop characteristics of control valves",
Applied Thermal Engineering, Elsevier.